Effect of the Austenitizing Temperature on Microstructure Evolution and Impact Toughness of a Novel Bainite Ductile Iron

Yongjin Wang[1] · Yingchao Zhang[1] · Renbo Song[1] · Liang Huang[1] · Yu Pei[1]

Abstract

The effect of austenitizing temperature on microstructure evolution and impact toughness of a newly developed Fe–3.0C–2.8Si–2.0Mn–0.9V–0.2Cr bainite ductile iron was investigated in this research. The ductile iron specimens were heat treated under different continuous cooling process, involving austenitizing between 900 and 980 °C and followed tempering at 200 °C. Optical microscopy, X-ray diffraction, scanning electron microscope and transmission electron microscope tests were conducted to investigate the microstructure evolution. Impact toughness and Rockwell hardness were measured. The results showed that the microstructure of the ductile iron mainly consisted of graphite, acicular bainite and retained austenite after continuous cooling process. The austenitizing temperature could change the volume fraction and size of bainite and retained austenite. There existed a C-area, where retained austenite accumulated near the graphite, except for specimen austenitized at 920 °C. The impact toughness of specimens increased first and then get worse with the increasing of austenitizing temperature. The impact toughness was related with the volume fraction of bainite and the morphology of retained austenite. The fracture mechanism of the bainite ductile iron belonged to cleavage fracture. Chunky graphite acted as the source of microcrack during the impact process. The bulky retained austenite behaved as a prior path for the microcrack propagation, while the bainite and thin filmy retained austenite limited its propagation.

Keywords Ductile iron · Bainite · Retained austenite · Impact toughness

1 Introduction

Ductile iron has been used in many areas as a substitute for cast and forged steels due to the good castability, excellent fatigue strength, remarkable fracture toughness, and low cost [1–4]. The mechanical properties of ductile iron are determined by the microstructure, consisting of graphite, ferrite, austenite, bainite, martensite or precipitates, etc. [5]. The bainite ductile iron demonstrates excellent combination of strength and toughness and is widely used in railroad, automotive, agricultural machinery, earth moving machinery, etc. [6, 7].

The bainite ductile iron is mainly obtained by isothermal quenching process in industry, while a few parts are produced by continuous cooling process [8]. The ductile iron, obtained by isothermal quenching process, is called austempered ductile iron (ADI). The ductile iron is heated above the lower critical temperature for austenitizing, followed by austempering at a temperature above the martensite start temperature (M_s). Bainite transition occurs during the isothermal process and the acicular bainite and high-carbon retained austenite are obtained. In order to obtain better mechanical properties, many researchers have studied the mixed structure consisting of pro-eutectoid ferrite and bainite, which are produced by intercritical austempering [9, 10]. But high amount of energy consumption is required during the isothermal process and the use of molten nitrate can also bring environmental problems. Many researchers pay attention to the continuous cooling process of bainite ductile iron.

The continuous cooling bainite ductile iron is obtained by heating above the upper critical temperature, followed by quenching to ambient temperature and then tempering at low

✉ Yongjin Wang
    wangyongjin@ustb.edu.cn

✉ Renbo Song
    songrb@mater.ustb.edu.cn

1   School of Materials Science and Engineering, University
    of Science and Technology Beijing, Xueyuan Road 30,
    Beijing 100083, China

temperature. Isothermal process is eliminated and the energy consumption is reduced. For the continuous cooling ductile iron, the control of hardenability brings several requirements such as chemical composition, cooling rate, size effect, etc. Sun et al. [8] investigated phase transformation of novel bainite ductile iron grinding balls by continuous cooling process. The result indicates that there were strong influences of austenitizing temperature and Jominy distance (D_J) on the cooling rate. Li et al. [11] fabricated a bainite-austenite ductile iron by designing the chemical composition and hardenability. The mechanical properties of the continuous cooling bainite-austenite ductile iron could reach the level of ADI. Zhou et al. [12] studied a wear resistant bainite-martensite ductile iron grinding ball. This material performed good impact abrasive wear resistance due to the presence of bainite, martensite and retained austenite. Previous work showed that the lower bainite and retained austenite were more beneficial to improve the properties of the ductile iron rather than the upper bainite [13].

As compared with ADI, the investigations of ductile iron fabricated by continuous cooling are relatively rare. The chemical composition and effect of continuous cooling parameters should be concerned [14, 15]. A reasonable chemical composition assures the hardenability of the continuous cooling ductile iron. Numerous studies have been conducted to focus on the performance of ductile iron such as tensile strength, fracture toughness and wear resistance. However, there is no in-depth research on the microstructure evolution during the austenitization. Besides, ductile iron is widely used under impact load state and the impact fracture mechanism should be clarified. In this paper, a novel Fe–3.0C–2.8Si–2.0Mn–0.9V–0.2Cr ductile iron is designed and the effect of austenitizing temperature on the microstructure evolution and impact toughness is investigated. The relationship between microstructure and mechanical properties is also revealed.

2 Experimental Procedure

In this study, a novel ductile iron is designed and the chemical composition is shown in Table 1. In commercial grade ductile cast iron, the content of Mn is generally not more than 0.7 wt%, and the content of Si is less than 2.5 wt%. But in the novel ductile iron, the content of the cheaper alloying element (Si and Mn) is 2–4 wt%. The Si and Mn can help improve the hardenability during continuous cooling. V is added to help refine the microstructure and form small precipitates.

The ductile iron was melted in a 15 kg medium frequency induction furnace. The melt was kept at 1450 °C for 3 min, and then was treated with 2.0% QRMg8RE3 for spheroidization

and 1.6% FeSi75 for inoculation. By pouring the melt into metal mold, it could produce the ball with 100 mm dimeter. Once solidified, the as-cast specimens were machined from the ball for subsequent test and heat treatment.

The specimens were heat treated under different austenitizing temperatures. They were heated at 900, 920, 940, 960, 980 °C for 2 h, followed by continuous cooling in solution of 15% NaCl+85% H_2O at ambient temperature. Subsequently, in order to release the residual thermal stress, they were tempered at 200 °C for 2 h, and then air cooled to ambient temperature. Rockwell hardness measurements were performed by using an Automatic Rockwell Hardness Tester. The impact tests were conducted on ZBC2452-B impact testing machine. Unnotched Charpy specimens of $10 \times 10 \times 55$ mm were machined. Three specimens were tested from each heat-treated condition and the average value was calculated.

Microstructure analyses were carried out on specimens from different heat treatment parameters to verify the effect of austenitizing temperature. The specimens were etched with 4% Nital solution. They were observed by the optical microscope (OM) and transmission electron microscope (TEM). The size and nodularity of graphite was calculated by following the standard of GB/T 9441-2009. Equations (1) and (2) were used to calculate the size and nodularity of graphite.

$$D = \frac{\sum_1^X \sqrt{4A/\pi}}{X} \tag{1}$$

$$N = \frac{1}{\left(\sum_1^X P^2/4\pi A\right)/X} \tag{2}$$

where D, N, A, X and P are average size, nodularity, area, the number and perimeter of graphite, respectively.

X-ray diffraction (XRD: Rigaku SmartLab, Cu target, operated at 40 kV and 150 mA with scanning speed 20°/min) analysis was performed to estimate the volume fraction of retained austenite and bainite. They were determined by comparison method using the integrated intensities of {200}, {220}, {311} austenitic peaks and {200}, {211} ferritic peaks according to the standard of YB/T5338-2006. The carbon content of the retained austenite (C_γ) was determined by the Eq. (3) [16].

$$A_\gamma = 3.548 + 0.00441C_\gamma \tag{3}$$

where A_γ is the lattice parameter of austenite in XRD results and C_γ is the carbon content of retained austenite.

After the impact tests, the fracture surface of each specimen was observed by scanning electron microscope (SEM)

Table 1 Chemical composition of ductile iron (wt%)

C	Si	Mn	V	Cr	Mg	RE	P	S	Fe
3.0	3.8	2.0	0.9	0.2	0.035	0.038	0.016	0.0041	Bal

along with Energy Dispersive X-ray Spectroscopy (EDS). Meanwhile, small slices cut from the perpendicular direction of fracture surface were used to observe the microcracks.

3 Result and Discussion

3.1 Microstructure Characterization of As-Cast Ductile Iron

Figure 1 shows the microstructure of specimens after polishing and 4% Nital etching, respectively. The volume fraction, mean size and nodularity of graphite can be calculated from Fig. 1a. Table 2 shows a summary of characterization for the as-cast ductile iron. The graphite appears the coexistence of spheroidal and chunky shape with nodularity of 71%. The volume fraction and mean size of graphite are 4.7% and 14.6 μm, respectively. The microstructure of the as-cast ductile iron is composed of lamellar pearlite and ferrite as shown in Fig. 1b. The volume fraction of ferrite and perlite are 24% and 71.3%, respectively. The average hardness of as-cast specimen is 44.1 HRC, while the average impact toughness is 2.9 J/cm^2. Obviously, the mechanical properties of as-cast ductile iron are poor and cannot meet the requirements of industrial production. Therefore, ductile iron must undergo subsequent heat treatment to improve the mechanical performance.

3.2 Effect of Austenitizing Temperature on the Microstructure of Ductile Iron

Figure 2 shows the microstructure of the specimens austenitized at 900, 920, 940, 960, 980 °C and tempered at 200 °C.

The microstructure mainly consists of graphite, acicular bainite and retained austenite for all specimens, which is different from the as-cast state. The volume fraction of graphite shows a decreasing trend with the increase of austenitizing temperature as shown in Table 3. It is observed that the shape of acicular bainite becomes coarser with the increase of austenitizing temperature. Figure 3 shows the TEM micrographs and selected area diffraction pattern (SADP) of the typical microstructures of specimens austenitized at 920 °C and 960 °C. Two kinds of austenite could be observed in the ductile iron. Figure 3a shows the thin filmy retained austenite and bainite laths in the specimen austenitized at 920 °C. Figure 3b shows the bulky retained austenite with a plenty of twins in the specimen austenitized at 960 °C. The bainite and austenite matrix could be also confirmed by the coexistence of these two peaks in XRD results shown Fig. 4. As the austenitizing temperature increases from 900 to 980 °C, the volume fraction of retained austenite decreases from 20.2 to 8.62% and then increases to 23.14% (Table 3). In the process of high temperature austenitization, the austenite grows up along the boundary of prior pearlite and ferrite, gradually occupies this part of the region and expands into ferrite to complete the final austenite transformation. After continuous cooling and tempering, some of the high temperature austenite is transformed into bainite and some is retained as austenite. As can be seen from Fig. 2a, c, d and e, there are some regions, where bulky retained austenite accumulates near the graphite, named as the C-area. However, the C-area is almost invisible in Fig. 2b. More small graphite nodules could be observed in Fig. 2b.

The volume fraction of retained austenite and dissolved carbon content in retained austenite was determined by XRD analysis. The influence of austenitizing temperature

Fig. 1 The as-cast microstructure of ductile iron: **a** polished specimen, **b** 4% Nital etched specimen
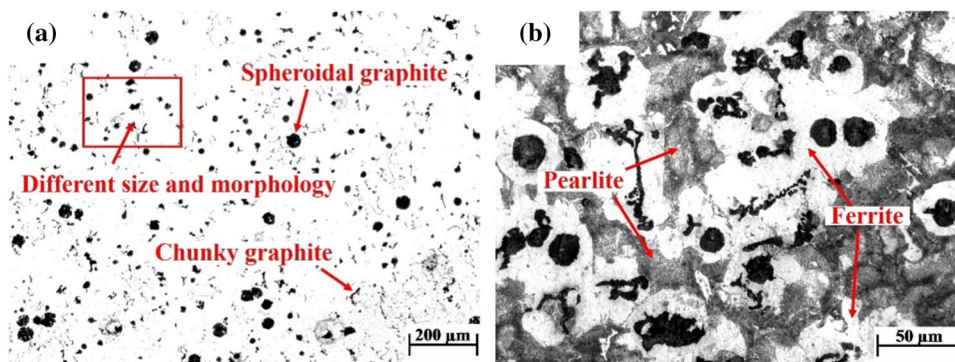

Table 2 Summary of characterization for the as-cast ductile irons

Volume fraction of graphite (%)	Size of graphite (μm)	Nodularity (%)	Volume fraction of ferrite (%)	Volume fraction of perlite (%)	Rockwell hardness (HRC)	Impact toughness (J cm^{-2})
4.7	14.6	71	24	71.3	44.1	2.9

Fig. 2 Microstructure of the ductile iron after austenitizing at **a** 900 °C, **b** 920 °C, **c** 940 °C, **d** 960 °C, **e** 980 °C and tempering at 200 °C
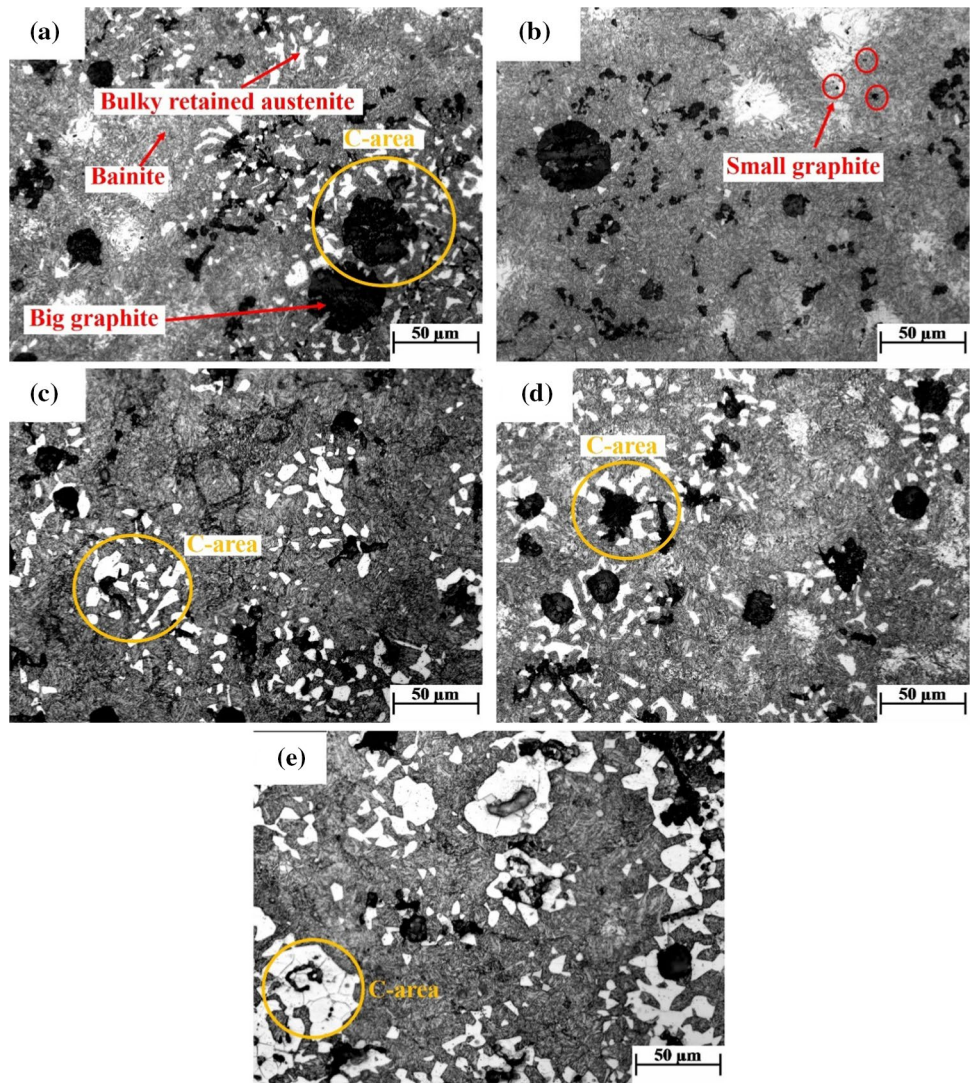

Table 3 Changes of the main phases with austenitizing temperatures

Austenitizing temperature (°C)	900	920	940	960	980
Volume fraction of graphite (%)	4.75	4.20	4.10	3.68	3.60
Volume fraction of retained austenite (%)	20.20	8.62	10.55	15.41	23.14
Volume fraction of bainite (%)	75.05	87.17	85.35	79.93	73.26

Fig. 3 The TEM micrographs and selected area diffraction pattern (SADP) of specimens austenitized at 920 °C (**a**) and 960 °C (**b**) and tempering at 200 °C
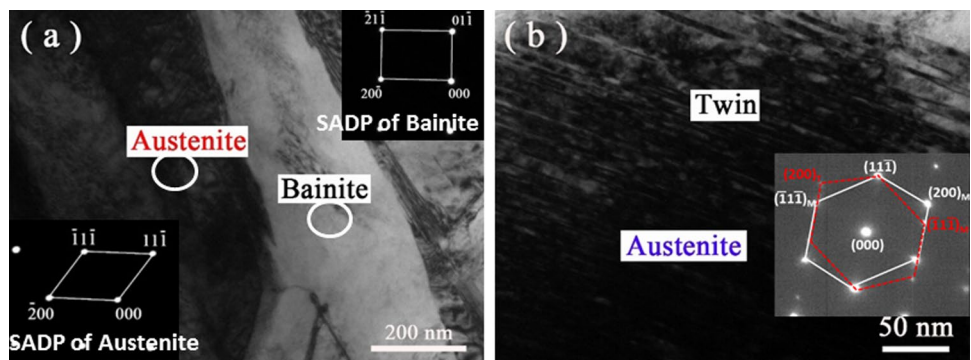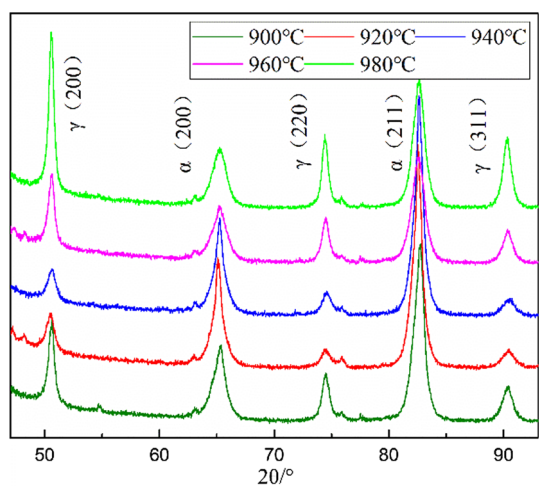
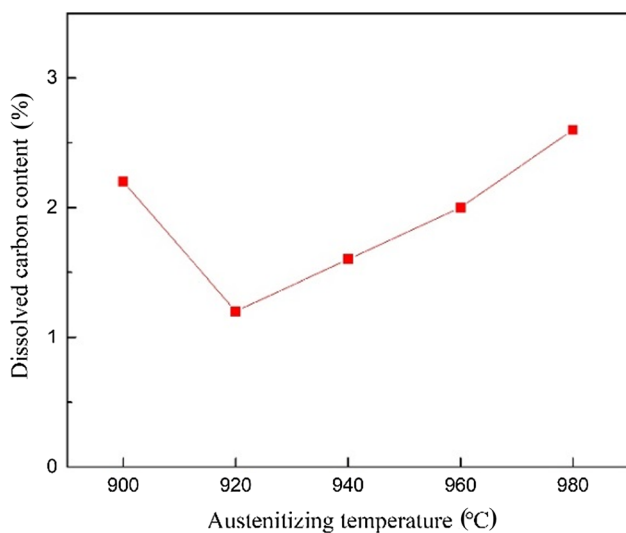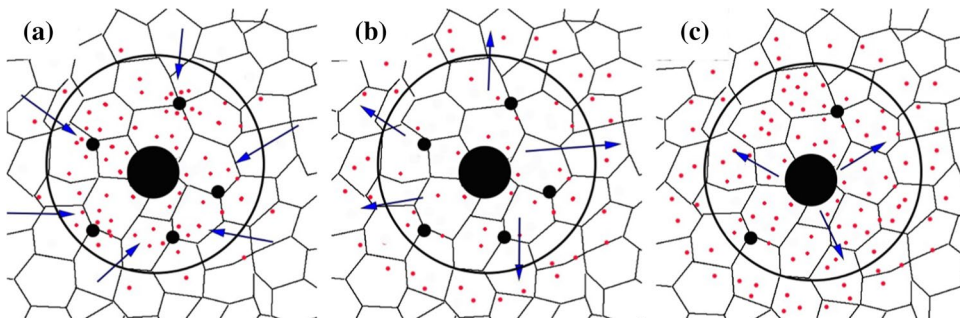**Fig. 4** XRD curves of ductile iron after austenitizing at 900–980 °C and tempering at 200 °C

Fig. 5 Changes of the dissolved carbon content of retained austenite with austenitizing temperature

could be observed in Table 3 and Fig. 5, respectively. At the austenitizing temperature range, the lowest volume fraction of retained austenite is 8.62% for the ductile iron

specimen austenitized at 920 °C. When the temperature exceeds 920 °C, the volume fraction and carbon content of austenite increase significantly. During the austenitizing process of ductile iron, the carburization of matrix is inevitable. The dissolution of carbon is related with the austenitizing temperature and austenitizing time. In a certain austenitizing time, high temperature leads to the fast dissolution of carbon into the matrix and the higher the concentration after reaching equilibrium [17]. The carbon in the retained austenite mainly comes from the pearlite of the as-cast, and some comes from the dissolution of graphite. Basso et al. [18] investigated the phase transformation in ductile iron occurring within the intercritical interval. The results showed a strong dependence between the alloy composition and the characteristics of the austenitization reaction.

Figure 6 is a schematic illustration of the diffusion and distribution of carbon atoms at different temperatures. When the specimen is austenitized at 900 °C, after decomposition of cementite, the carbon atom has enough time to diffuse through the boundary of austenite grain and the internal defects of the crystal to the original graphite. Therefore, carbon atoms keep accumulating and the carbon content increases in the C-area, as shown in Fig. 6a. When the austenitizing temperature increases up to 920 °C, the carbon solubility of austenite also increases. The carbon atoms begin to diffuse towards the outside region, and the carbon content is reduced in C-area as shown in Fig. 6b. When the austenitizing temperature continues to rise, the small graphite gradually dissolves and becomes smaller, and the carbon content in C-area gradually increases as shown in Fig. 6c. Therefore, the carbon content of retained austenite is directly related with the austenitizing temperature [19, 20]. The lower austenitizing temperature is beneficial to the formation and growth of graphite. At high austenitizing temperature, the small graphite becomes smaller due to dissolution. As the austenitizing temperature improves, the carbon content of retained austenite decreases firstly and increases subsequently, which determine the stability of supercooled austenite. So, when the specimen is heated at 920 °C, the volume fraction of retained austenite is lowest.

Fig. 6 Schematic illustration of the diffusion and distribution of carbon atoms of specimens austenitized at **a** 900 °C, **b** 920 °C, **c** 980 °C (Black dots: different sizes of graphite, red dots: carbon atoms, black circles: C-area, blue arrows: directions that carbon atoms diffuse)

3.3 Effect of Austenitizing Temperature on the Mechanical Properties of Ductile Iron

Figure 7 shows the mean values of Rockwell hardness of specimens after quenching and tempering. The hardness of specimens is improved by 17%–21% after heat treatment as compared with the as-cast ductile iron. The significant increase is mainly due to the transformation from ferrite and pearlite at the as-cast state into bainite and retained austenite. TEM analysis shows that nano-sized carbides appear in the matrix, as shown in Fig. 8. This carbide is present in the form of a single vanadium-containing particle according to EDS results and the vanadium carbide may help improve the hardness. Higher temperature is more likely to make the carbides or graphite to dissolve and then increases the carbon content in the matrix, which has been confirmed in Fig. 5. When austenitizing temperature increases, the hardness of the matrix gradually improves with the dissolution of more alloying elements.
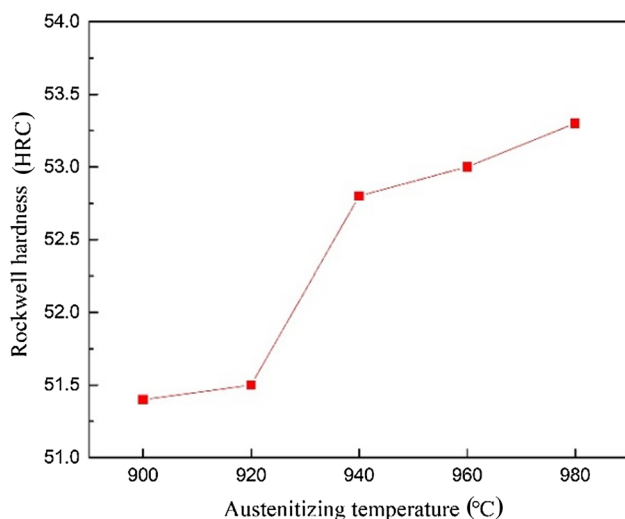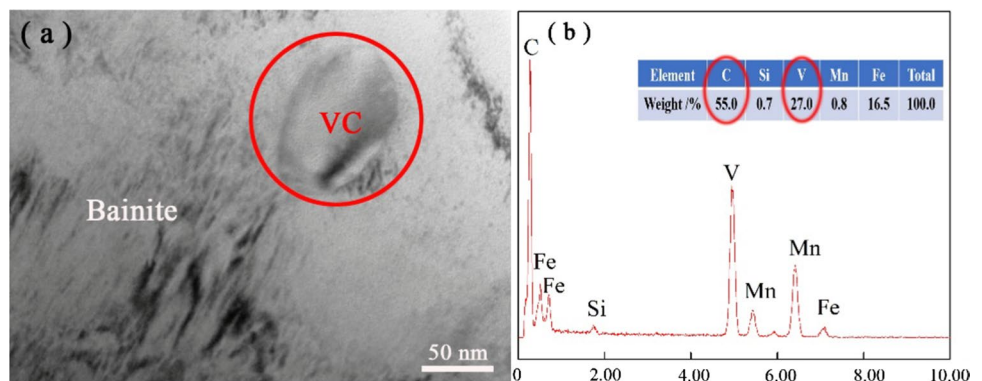
Figure 9 shows the impact results of the specimens after heat treatment. The impact toughness of the continuous cooling ductile iron improves significantly as compared with the as-cast specimen. The improvement in impact toughness is mainly due to the difference in the microstructure. The microstructure of as-cast ductile cast iron is mainly composed of pearlite, ferrite and graphite. And it is inevitable that the micro-segregation exists in the as-cast microstructure, which leads to a decrease in the uniformity of the as-cast and is bad for the toughness. After proper heat treatment, the microstructure of the ductile iron is acicular bainite, retained austenite, and graphite. The bainite contributes to improve hardness and toughness and the retained austenite is also good for toughness. The microstructure can obviously improve the comprehensive performance. As the austenitizing temperature improves, the impact toughness increases first and then gets worse, which is consistent with the change of volume fraction of bainite as shown in Table 3. As compared with the specimens austenitized at 900 °C and
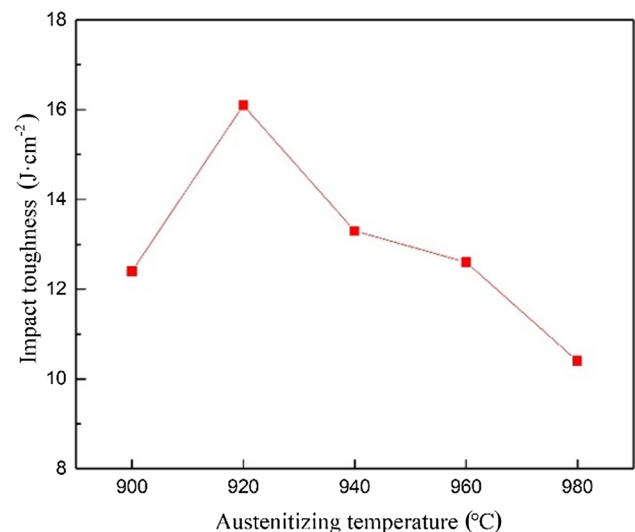
Fig. 7 The mean values of Rockwell hardness of specimens after quenching and tempering

Fig. 9 Changes of the impact toughness value as a function of temperature

Fig. 8 a TEM micrograph and **b** EDS results of VC carbide

980 °C, the impact toughness of specimens austenitized at 920 °C was improved by 58% and 31%, respectively. Figure 9 and Table 3 indicate that bainite enhances the ductility of ductile iron. So, it is important to make an intensive study of this phenomenon via the fracture analysis.

3.4 Impact Fracture Mechanism

Figure 10 shows fracture surface of the specimen austenitized at different temperatures. The fracture surface is rough and the whole fracture is uneven. Due to the incongruity of the deformation between the graphite and the matrix, the graphite and the matrix are separated under the impact force. The separation of graphite from the matrix leaves some holes. There are a lot of cleavage steps, microcracks and tearing ridges on the fracture surface. The tearing ridges are formed by tearing around the graphite, which can improve the resistance of microcrack generation and propagation. The fracture mechanism of the bainite ductile iron is

cleavage fracture. At lower or higher temperatures of 900 °C or 980 °C, there are many cracks on the fracture surface as shown in the Fig. 10a and e, which leads to the low impact toughness.

In order to clarify the crack propagation path, the longitudinal plane of impact fracture is observed by SEM as shown in Fig. 11. It is found that the graphite plays an important role in the initiation of microcrack during fracture. The microcracks mainly occurs around chunky graphite and extends along the matrix to the next chunky graphite. Therefore, it can be considered that the sharp angle of these chunky graphite acts as the source of microcrack during the impact process. Meanwhile, Foglio et al. [21] concluded that the prime influence of chunky graphite was the preferential path for microcrack propagation. As shown in Fig. 11c, when the crack is generated, it is more likely to spread to the adjacent retained austenite rather than the adjacent bainite, and it will stop at the phase boundary between them. The impact toughness increases with the bainite content. More

Fig. 10 Fracture surfaces of the impact test specimens austenitized **a** 900 °C, **b** 920 °C, **c** 940 °C, **d** 960 °C, **e** 980 °C and tempering at 200 °C
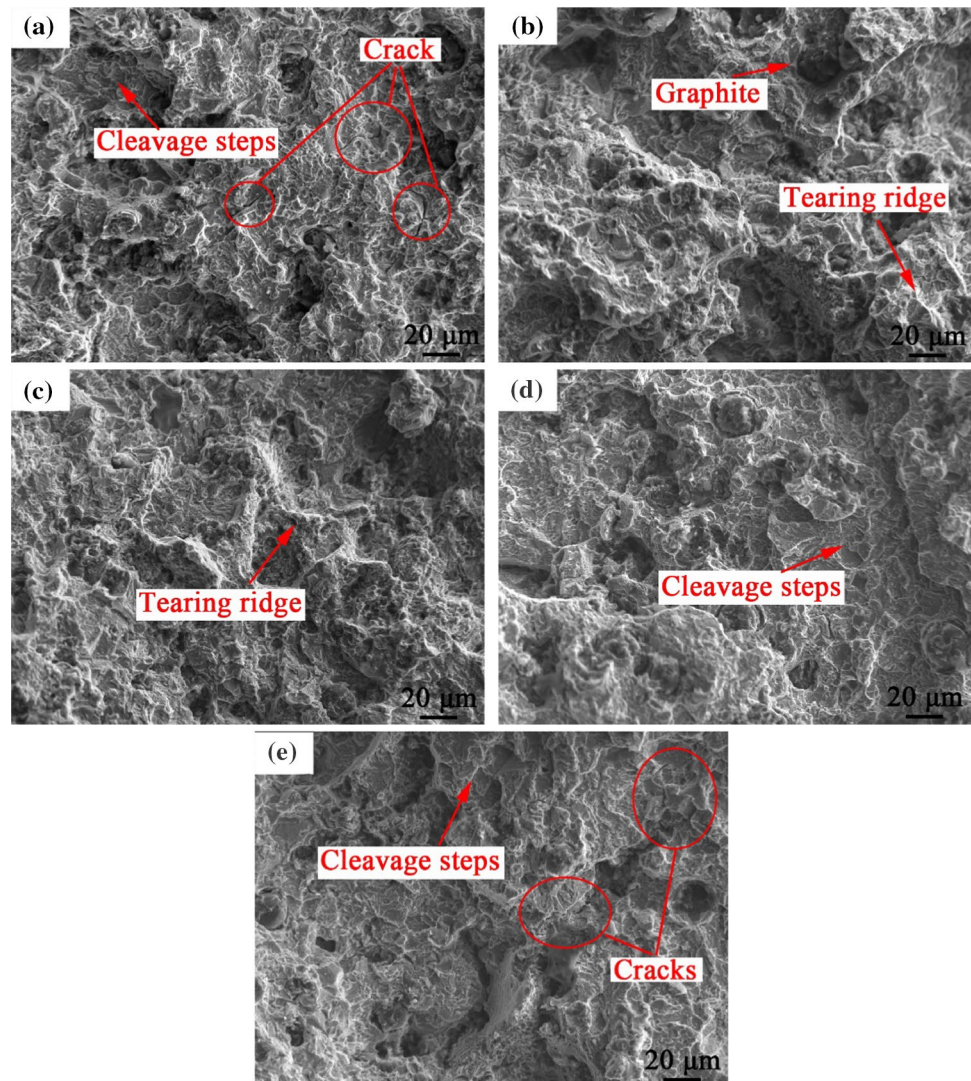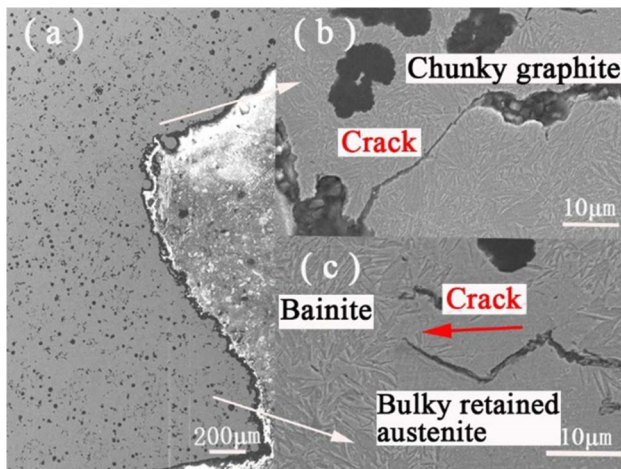
Fig. 11 SEM image of fractured specimen along the longitudinal plane: **a** fracture morphology, **b** the microcrack propagated between the graphite, **c** the crack ended in the bainite

Fig. 12 Microcosmic diagram of crack propagation in ductile iron (G: graphite; A: thin filmy retained austenite; B: bainite)

retained austenite leads to the lower impact toughness. This is obviously inconsistent with the traditional conclusion that retained austenite can improve the toughness of materials [22]. Miihkinen' work showed the bulky retained austenite had less mechanical and thermal stability, leading to the decrease of toughness [23]. The crack occurred at the tip of the graphite and then propagated to the material matrix. As shown in Fig. 12, when the thin filmy retained austenite and bainite exist layer by layer, the microstructure characterization would constrain the growth of the crack. However, it is easier for the cracks to expand in bulky retained austenite. The bulky retained austenite seems to be a preferential path for the crack propagation in comparison with bainite.

4 Conclusions

(1) The microstructure of the ductile iron mainly consists of graphite, acicular bainite and retained austenite after continuous cooling process. The hardness and impact toughness of the ductile iron are improved by at least 7.5 HRC and 7.4 J/cm^2 due to the excellent properties of bainite.

(2) The austenitizing temperature can change the volume fraction and size of bainite and retained austenite. There exists a C-area, where retained austenite accumulates near the graphite, except for specimen austenitized at 920 °C.

(3) The impact toughness of specimens increases first and then gets worse with the increasing of austenitizing temperature. The impact toughness is related with the volume fraction of bainite and the morphology of retained austenite.
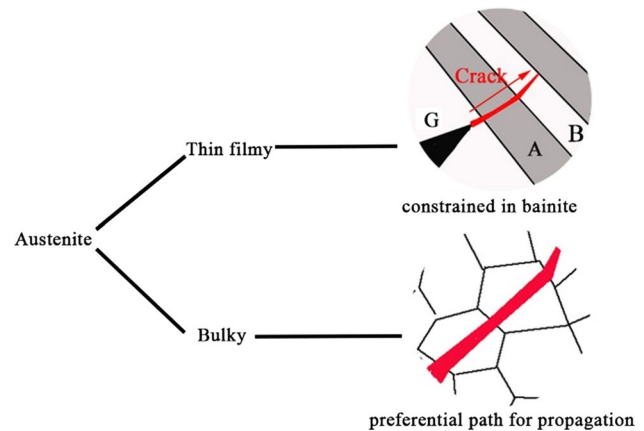
(4) The fracture mechanism of the bainite ductile iron belongs to cleavage fracture. Chunky graphite acts as the source of microcrack during the impact process. The bulky retained austenite behaves as a prior path for the microcrack propagation, while the bainite and thin filmy retained austenite limit its propagation.

References

1. X. Chen, J. Xu, H. Hu, H. Mohrbacher, M. Kang, W. Zhang, A. Guo, Q. Zhai, Mater. Sci. Eng. A **688**, 416 (2017)
2. T. Borsato, P. Ferro, F. Berto, C. Carollo, Int. J. Fatigue **102**, 221 (2017)
3. J.F. Dias, G.O. Ribeiro, D.J. Carmo, J. Vilela, Mater. Sci. Eng. A **556**, 408 (2012)
4. S. Laino, J.A. Sikora, R.C. Dommarco, Wear **265**, 1 (2008)
5. A.D. Basso, R.A. Martinez, J.A. Sikora, Mater. Sci. Technol. **23**, 1321 (2007)
6. H. Zhang, Y. Wu, Q. Li, X. Hong, Wear **406**, 156 (2018)
7. A. Sinlah, D. Handayani, R.C. Voigt, K. Hayrynen, R. M'Saoubi, C. Saldana, J. Cast Metal. Res. **29**, 62 (2016)
8. T. Sun, R. Song, X. Wang, P. Deng, C. Wu, Mater. Sci. Eng. A **626**, 375 (2015)
9. S.C. Murcia, M.A. Paniagua, E.A. Ossa, Mater. Sci. Eng. A **566**, 8 (2013)
10. J. Aranzabal, G. Serramoglia, C.A. Goria, D. Rousière, Int. J. Cast Metal. Res. **16**, 185 (2003)
11. J.Z. Li, X.S. Ning, W.H. Lu, Q.D. Zhou, Stren. Met. Alloys. **3**, 1311 (1989)
12. R. Zhou, Y. Jiang, D. Lu, R. Zhou, Z. Li, Wear **250**, 529 (2001)
13. M. Soliman, H. Ibrahim, A. Nofal, H. Palkowski, J. Mater. Process. Tech. **227**, 1 (2016)

14. P. Weiß, A. Tekavčič, A. Bührig-Polaczek, Mater. Sci. Eng. A **713**, 67 (2018)
15. A. Alhussein, M. Risbet, A. Bastien, J.P. Chobaut, D. Ballou, J. Favegeon, Mater. Sci. Eng. A **605**, 222 (2014)
16. C.S. Roberts, Trans. AIME. **197**, 203 (1982)
17. M. Górny, G. Angella, E. Tyrała, M. Kawalec, S. Paź, A. Kmita, Met. Mater. Int. **25**, 956 (2019)
18. A. Basso, R. Martínez, J. Sikora, J. Alloy. Compd. **509**, 9884 (2011)
19. A.S. Nishikawa, G. Miyamoto, T. Furuhara, A.P. Tschiptschin, H. Goldenstein, Acta Mater. **179**, 1 (2019)
20. S. Panneerselvam, S.K. Putatunda, R. Gundlach, J. Boileau, Mater. Sci. Eng. A **694**, 72 (2017)
21. E. Foglio, D. Lusuardi, A. Pola, G. Vecchia, M. Gelfi, Mater. Design **111**, 353 (2016)
22. J. Yang, S.K. Putatunda, Mater. Sci. Eng. A **393**, 254 (2005)
23. V.T.T. Miihkinen, D.V. Edmonds, Mater. Sci. Technol. **3**, 441 (2013)